JOURNAL OF SOLID STATE CHEMISTRY 55, 133–149 (1984)

Structure Models for β-$MnGa_2S_4$ as Derived from Electron Diffraction and High-Resolution Electron Microscopy

M. DE GRAEF,*,** M. BAKKER,*,† M. VAN HEMERT,*,‖
J. VAN LANDUYT,‡ AND S. AMELINCKX‡,§

Gorlaeus Laboratory of Inorganic Chemistry, University of Leiden, The Netherlands; ‡University of Antwerp, RUCA, Groenenborgerlaan 171, B-2020 Antwerp, Belgium; and §SCK–CEN, B-2400 Mol, Belgium

Received March 7, 1984

A study by high-resolution electron microscopy and electron diffraction on the tetrahedrally coordinated compound β-$MnGa_2S_4$ is reported. The structure-imaging technique enabled a new structure model to be proposed for the accommodation of deviations from stoichiometry in compounds of the type $xMnS/yGa_2S_3$. The model is based on the Ga_2S_3 structure wherein by the substitution of MnS layers chemical twin planes are formed. Depending on the spacing of the periodic twin planes a homologous series of compounds is expected and a number of members of this series was identified mainly by electron diffraction. In the β-$MnGa_2S_4$ compound, two structure modifications are observed mainly differing in the orientation of the twin planes (coherent or incoherent). This conclusion is substantiated by structure image calculations for the interpretation of the high-resolution results.

1. Introduction

It has become clear in recent years that deviations from composition in more or less ionic octahedral compounds are often associated with the occurrence of extended defects such as crystallographic shear planes or mimetic twins (*1, 2*). Also the fine-scale intergrowth of two or more structures is reported as a means by which composition variations are accommodated (*2, 3*).

Little knowledge exists about the accommodation of nonstoichiometry in tetrahedral compounds with mainly covalent bonding. Interesting are the compounds based on a hcp or ccp stacking, for which the structures can be derived from the Wurtzite- or Blende-type structure. In these structures all atoms are tetrahedrally surrounded: in ZnS each Zn is surrounded by four S atoms, and each S by four Zn atoms. In the so-called defect-tetrahedral structures one of the atoms is bonded to less than four other atoms. These compounds can be thought to be derived from the Wurtzite- or Blende-type structures by a substitution through which vacancies are introduced (*4*), for example, $3A^{2+} \rightarrow 2B^{3+}$ + 1 vacancy where A and B represent divalent and trivalent cations, respectively. For a number of defect tetrahedral compounds; disorder and phase regions of nonstoichiometry are reported (*4*). In (*5*) the system MnS–Ga_2S_3 was investigated in order

** Present address: Department Metaalkunde en Materiaalkunde, De Croylaan 2, B-3030 Heverlee, Belgium.

† Present address: OCE Vandergrinten, Venlo, The Netherlands.

‖ Present address: Vakgroep Anorganische Chemie en Materiaalkunde, Postbus 217, 7500 AE Enschede, The Netherlands.

0022-4596/84 $3.00

to find some structural principle that could enable one to understand these phenomena in this type of compounds. The present paper reports on the main results from (*5*) complemented by a structural study mainly on the β-$MnGa_2S_4$. A number of xMnS/$y$$Ga_2S_3$ samples were prepared and examined by means of X-ray powder diffraction, electron microscopy, and electron diffraction. High-resolution imaging and image computation were used to confirm the proposed structure models.

2. Structural Aspects

In the cubic ZnS (Blende) and hexagonal ZnS (Wurtzite) structures the metal atoms as well as the sulfur atoms have tetrahedral coordination. The unit cell dimensions of these parent structures are $a = 0.5493$ nm ($F43m$) and $a = 0.3811$ nm, $c = 0.6811$ nm ($P63mc$) (*6*). The present paper will deal with Wurtzite-type structures only.

In the system MnS · Ga_2S_3 a number of hexagonal-based tetrahedral compounds have been found as a result of extensive X-ray diffraction studies (*7, 8*). The compounds based on hcp in this system are Ga_2S_3, β-$MnGa_2S_4$ and three other compounds of which the structure and the unit cell dimensions are unknown: $MnGa_4S_7$, $MnGa_6S_{10}$, and $MnGa_8S_{13}$.

The powder diffraction studies furthermore showed a high solubility of MnS in Ga_2S_3, based on a random occupation of the tetrahedral sites. At a temperature of 973 K a solid solution region is formed up to the composition 1MnS · Ga_2S_3 (i.e., $MnGa_4S_7$). A solid solution of Ga_2S_3 in $MnGa_2S_4$ (*9*) results in a ccp structure.

The structure of β-$MnGa_2S_4$ (H.T.) is thought to be isostructural with β-$ZnAl_2S_4$ (*10*) ($(Pna2_1)$, $a = 1.282$, $b = 0.75$, $c = 0.609$ nm). This structure is supposed to be built of slabs of ordered and disordered structures along the c-axis.

The structure of α-Ga_2S_3 is monoclinic with unit cell dimensions $a = 1.1094$, $b = 0.6395$, $c = 0.9578$ nm, $\beta = 141.15°$, space group Cc (*11, 12*). The structure of β-Ga_2S_3, the high-temperature phase, is disordered with a Wurtzite-type structure (*13*). The ordered structure of α-Ga_2S_3 can be derived from the cubic ZnS structure by replacing three ZnS_4 by two GaS_4 tetrahedra plus one vacant site in an ordered manner. Within a close-packed plane (00.1) there are sequences of tetrahedral sites, *–Ga–Ga–*–Ga–Ga, etc. such that each vacant site (*) is surrounded by six filled tetrahedra. In Fig. 1 the structure is drawn, projected along the [10.0] direction; Ga-filled S tetrahedra are crosshatched. Stacking of the (00.1) planes as shown in the figure results in a monoclinic structure with unit cell $3a_h$, $a_h + 2b_h$, $-2a_h + c_h$ (*12*). Vacancies are situated in planes parallel to the $(100)_m$ planes as indicated by the dashed lines.

It is worth noticing that in the structure of Ga_2S_3 there are two types of sulfur polyhedra: two S atoms surrounded by three Ga atoms and one vacancy and one S atom surrounded by two Ga atoms and two vacancies. (The average number of valence electrons per Ga is $(2 \times (3 \times \frac{3}{4}) + (2 \times \frac{3}{4})) : 3 = 2$.) The latter S atoms clearly are short of electrons. Upon formation of anti-phase boundaries these S atoms will be located in

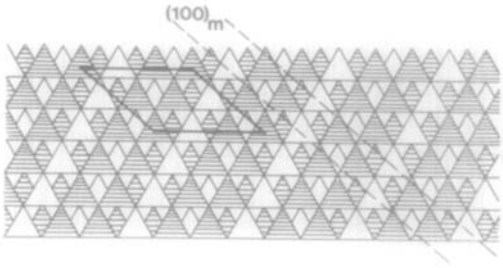

FIG. 1. The [10.0] projection of the Ga_2S_3 structure; the corners of the triangles represent sulfur atoms. Crosshatched triangles represent Ga-filled tetrahedra. The monoclinic unit cell is indicated by solid lines.

the less-dense atom planes and thus will be more scattered over the matrix structure.

3. Experimental

α-MnS was prepared from $MnCO_3$ in a r.f. induction furnace in a H_2S atmosphere contained in a graphite crucible. Ga_2S_3 was prepared by heating the metal in a graphite crucible under H_2S in the r.f. furnace at 1473 K; the result was a yellow powder. This powder was placed in a carbon crucible and reheated for 48 hr at 973 K under H_2S in a silica tube. The color then changed from yellow to gray. Mixtures of MnS and Ga_2S_3 in ratios of 1/1, 2/3, 3/4, 2/5, 1/3, 2/7, 1/4, and 1/5 were heated in the r.f. furnace to 1373 K for 20 min followed by a heat treatment during 24 hr at 1073 K, and air cooling. All samples appeared to have melted and resolidified. The process of instantaneous melting appeared fruitful as it prevented to a large extent the sublimation of Ga_2S_3. However, it was not possible to prevent this completely; the sample compositions will thus show minor deviations from the nominal compositions.

The powder diffraction pattern of Ga_2S_3 was recorded on a Philips powder diffractometer (Cu$K\alpha$, $\lambda = 0.15418$ nm), as well as for some heated mixtures. For examination in the electron microscope (Siemens Elmiskop 102) samples were obtained by crushing; thin flakes were dispersed in alcohol and mounted on a 400-mesh copper grid coated with a Formvar/carbon holey film. To be able to determine lattice constants with a good accuracy from the electron diffraction patterns, the camera length λL was calibrated versus the objective current, using an Al-film.

High-resolution observations were performed with a JEM 200 CX microscope equipped with a top-entry high-resolution stage with pole-pieces with a $C_s = 1.2$ mm. The obtainable resolution for structure imaging amounts to 0.26 nm. A double-tilt stage ($\pm 10°$) could be used for orienting the specimens along a zone axis.

4. Results

4.1. X-Ray Diffraction

The powder diffraction pattern obtained from the Ga_2S_3 sample was similar to the previously reported one (*11*). It was possible to identify this phase as α-Ga_2S_3 (monoclinic structure). Most obvious in the diffraction pattern are the reflections from the hcp basic Wurtzite-type structure, besides a number of broad additional reflections. The unit cell of the hcp structure was measured to be $a = 0.3695(1)$, $c = 0.6026(3)$ nm, $c/a = 1.631$. In this sample neither oxysulfide nor GaS nor metallic Ga could be detected. All the mixtures MnS/Ga_2S_3 gave very similar diffraction patterns. Besides the Wurtzite-type reflections, however, numerous weaker additional reflections also occur. The basic unit cell dimensions are $a = 0.371(1)$, $c = 0.606(1)$ nm, $c/a = 1.63$ in case of composition $1MnS/1Ga_2S_3$ and $a = 0.3719(1)$, $c = 0.6087(1)$ nm, $c/a = 1.637$ in case of composition $1MnS/5Ga_2S_3$. These results are in accordance with previously reported work on this system (*8*).

4.2. Electron Microscopy and Diffraction

Several selected area diffraction patterns, together with either bright- or dark-field images or lattice images along different crystallographic directions were obtained by the use of the double-tilt and lift device in the electron microscope. Mostly the crystals had to be tilted over large angles in order to obtain the reciprocal lattice sections with the highest symmetry, characteristic of the Wurtzite-type structure. The most typical diffraction patterns will be described hereafter. The Ga/Mn ratio increases in Figs. 3a to f.

Figure 2 shows two reciprocal lattice sec-

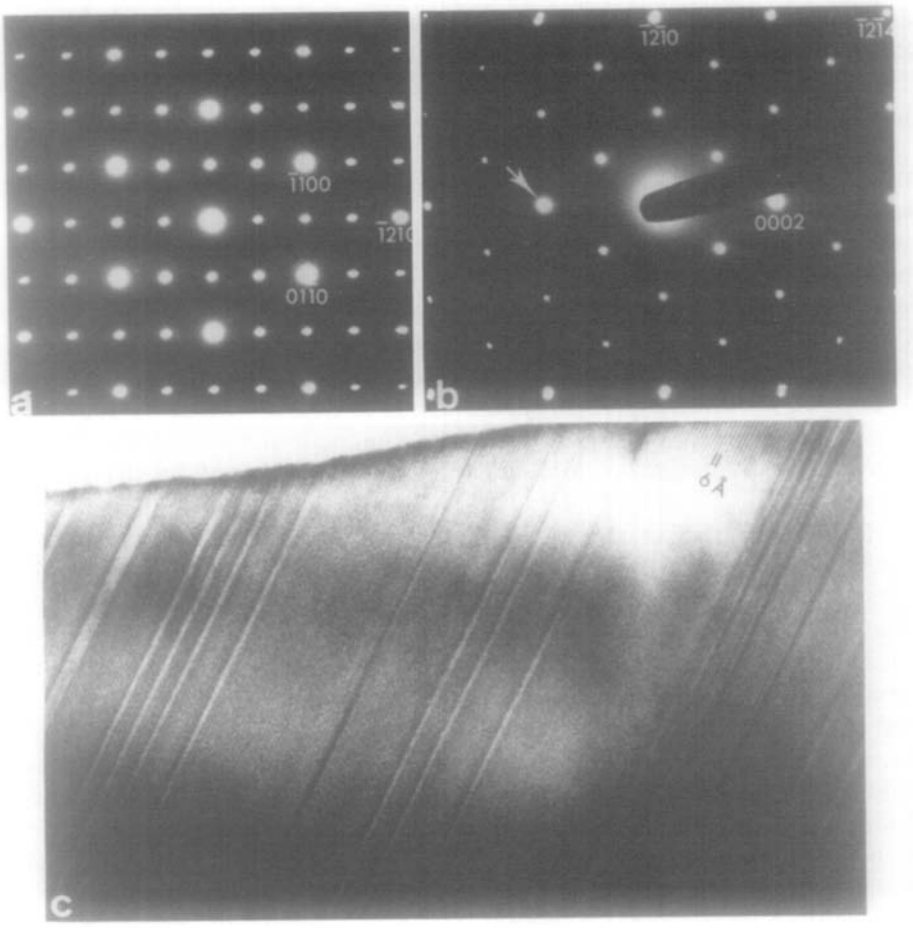

FIG. 2. Electron diffraction patterns and lattice image of $MnGa_2S_4$: (a) [00.1] section, (b) [01.0] section, and (c) lattice image using the transmitted beam and the beam indicated by an arrow in (b).

tions obtained from a sample with the composition $MnGa_2S_4$. The brightest spots originating from a Wurtzite-type matrix have been indexed. The unit cell dimensions were measured: $a = 0.370(2)$, $c = 0.612(3)$ nm, $c/a = 1.65$. Figure 2c shows the micrograph corresponding with Fig. 2b, in which several planar faults are visible. The [01.0] reciprocal lattice section, with its superreflections, is particularly important for the $MnS \cdot Ga_2S_3$ system, as in this section the changes resulting from the increase in the Ga/Mn ratio are most striking. In Fig. 3a, obtained from a sample MnS/Ga_2S_3: 3/4, besides the superreflections as in Fig. 2b, additional diffuse lines run in two symmetry-related directions $g(\bar{1}2.4)$. Within the diffuse lines distinct maxima occur: between the origin and the $(\bar{1}2.4)$ reflection there are six of these maxima. Note that in Fig. 2b the number of superreflections in this direction is 3. In the diffraction pattern of Fig. 3b the additional superreflections are stronger and sharper, whereas no diffuse lines are observed. Although the sample composition is MnS/Ga_2S_3: 2/3, diffraction patterns like Fig. 3a are also observed in this sample.

In Fig. 3c for the sample with composition MnS/Ga_2S_3: 2/5, the three superreflec-

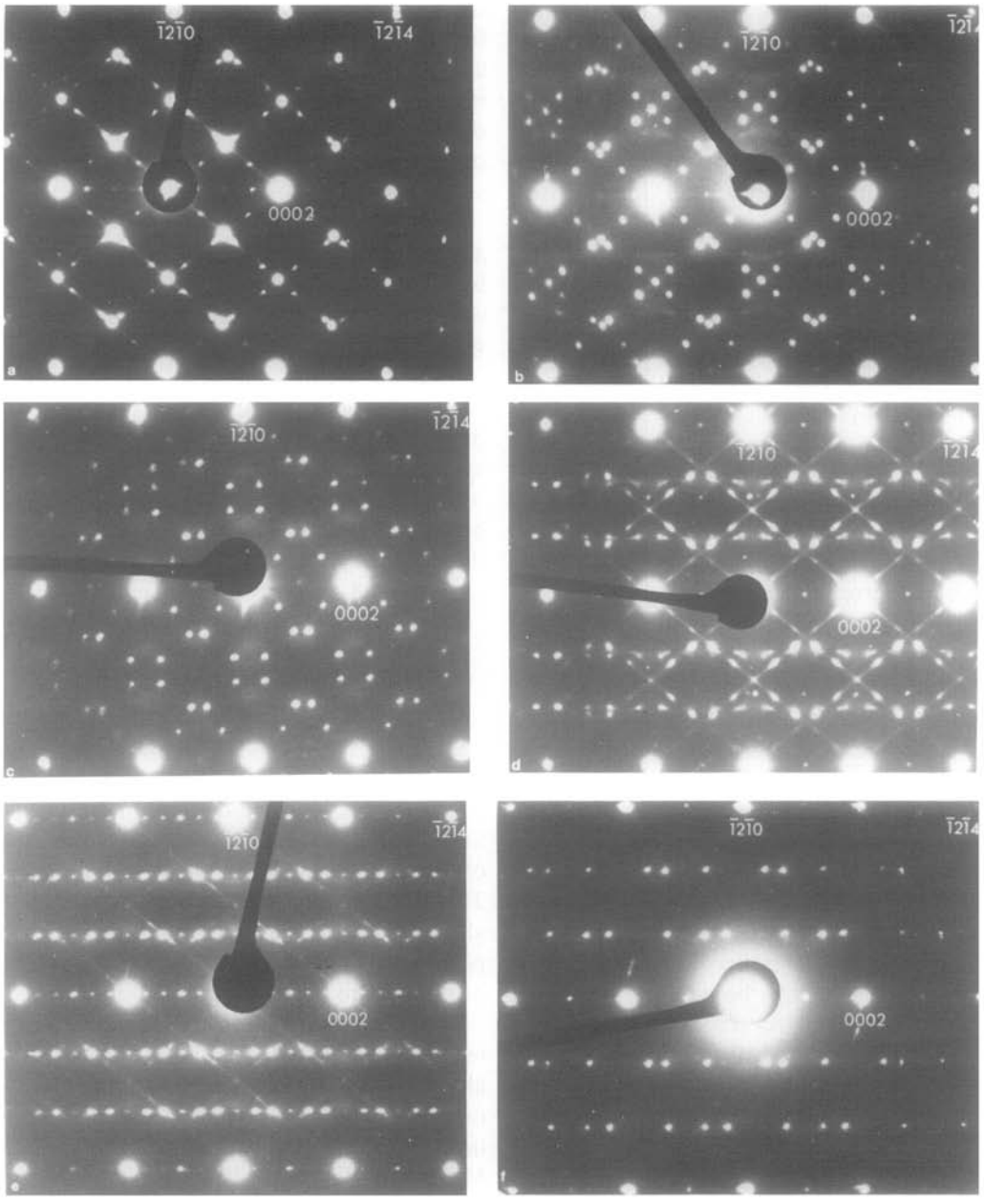

FIG. 3. The [01.0] reciprocal lattice section from samples $x Ga_2S_3$–$y MnS$ with increasing Ga/Mn ratio, from (a) to (f) (see text). Note that the number of superreflections along $g(\bar{1}2.4)$ changes with composition. Some patterns also show streaking along $g(\bar{1}2.4)$, (a), (d), and (e).

tions of Fig. 3a do no longer occur. In Fig. 3d with sample composition MnS/Ga_2S_3: 1/3 again diffuse streaks are visible along the two directions $g(\bar{1}2.4)$. Close inspection of the streaks reveals that now nine maxima occur between the origin and the $(\bar{1}2.4)$ reflection. Additional groups of spots becoming sharper at the edge of the Ewald sphere

are positioned at lines parallel to $g(00.2)$ and at 1/3 and 2/3 from the $(\bar{1}2.0)$ reflection. The diffraction patterns of Figs. 3e and f were both obtained from a sample with composition MnS/Ga_2S_3: 1/5. In both patterns new superreflections occur. Two extra reflections are observed in the two equivalent directions between the origin and the $(\bar{1}2.4)$ reflection. Between these rows, additional rows of superreflections are visible. These are not observed in the other diffraction patterns, although often the (00.1) reflection appears. This will be explained later.

5. Discussion

5.1. Compositions Ga_2S_3 and $MnGa_2S_4$

The superreflections in Fig. 2 can all be indexed using a supercell of the type $2a_h$, $a_h + 2b_h$, c_h (orthorhombic $a = 0.740$, $b = 0.639$, $c = 0.612$ nm) for a crystal with composition $MnGa_2S_4$. This unit cell is not of the type β-$ZnAl_2S_4$ (*10*) but of the type $BeSiN_2$ (*4*). The fact that the hcp matrix reflections are well defined and sharp in contrast to the streaked superreflections suggests that the planar faults (Fig. 2c) are anti-phase boundaries in the metal atom lattice and not stacking faults (mixed hcp and ccp) in the sulfur lattice. The diffraction pattern of Fig. 3f can be indexed using the reported unit cell for the structure of α-Ga_2S_3 (the calculated diffraction pattern is shown schematically in Fig. 4b except for the additional row of superreflections, which are forbidden ($l = odd$) in the space group Cc (*12*). This means that either the periodicity along $g(00.1)$ is doubled or that the reflection appears through a structural deformation. The latter possibility could explain the spots as follows: if a structural deformation changes the atom parameters for α-Ga_2S_3 to a structure with space groups $C2$ or Cm, the extra reflections with $l = odd$ are not forbidden. In this respect it is pertinent to remark that diffraction patterns obtained from crystals from the sample with composition MnS/Ga_2S_3: 1/5 using a high-intensity electron beam do not show the $l = odd$ reflections, while the superreflections of α-Ga_2S_3 (ordering of the tetrahedral sites) remain.

Another more plausible possibility is that a second structure variant is present to a limited extent which causes the weak $l = odd$ reflections. In a following section we will show that such a variant does exist.

The diffraction patterns for the [01.0] zones for β-$MnGa_2S_4$ and α-Ga_2S_3 are drawn schematically in Fig. 4b and a, respectively. Note that in this zone only one orientation variant of α-Ga_2S_3 within the hexagonal matrix has been drawn. In total there are 2×3 orientation variants for α-Ga_2S_3 and 3 variants for β-$MnGa_2S_4$.

5.2. Compositions Intermediate between Ga_2S_3 and $MnGa_2S_4$

A combination of diffraction patterns and dark-field images revealed that for $MnGa_2S_4$ and Ga_2S_3 deviations from stoichiometric composition result in the formation of new phases by coherent intergrowth of structural units of these compounds. This suggests that both structures are mutually related. Using this relationship it is possible to unravel the complicated series of diffraction patterns of Figs. 3a–f.

A common feature in the diffraction patterns is the number of superreflections along the two equivalent crystallographic directions $g(\bar{1}2.4)$. It is of course the ordering of the metal atoms in the compounds $MnGa_2S_4$ and Ga_2S_3 that causes the four- and threefold periodicity along $g(\bar{1}2.4)$ with reference to the hcp matrix. The seven- and tenfold periodicity is another type of metal-atom ordering that corresponds to new compounds. The preparation data of the investigated samples suggest that the compositions are $MnGa_4S_7$ and $MnGa_6S_{10}$. It should be mentioned that these composi-

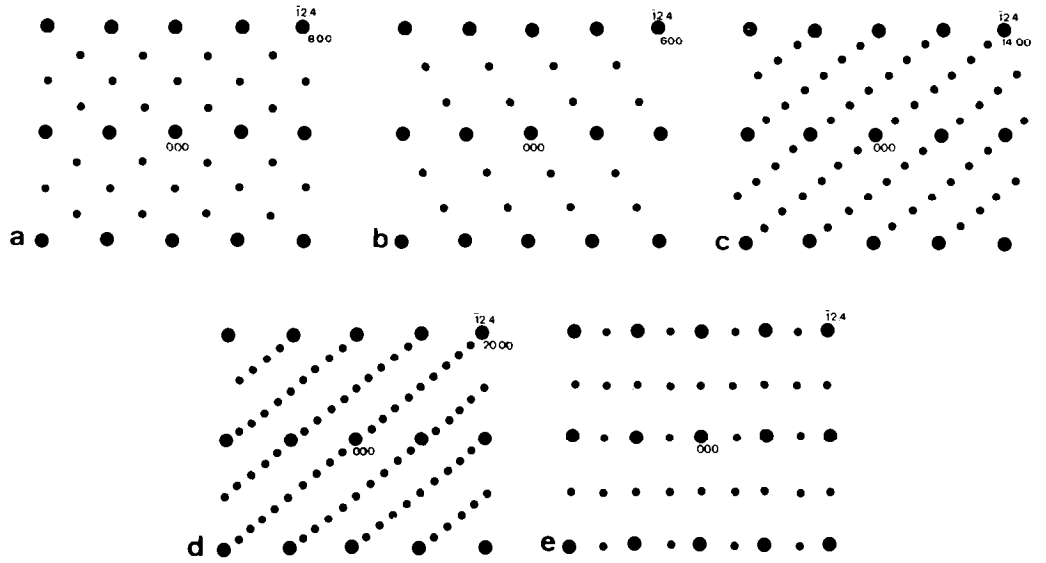

FIG. 4. Calculated diffraction patterns (schematic) for single domain variants of β-$MnGa_2S_4$ (a), α-Ga_2S_3 (b), $MnGa_4S_7$ (c), $MnGa_6S_{10}$ (d), and a second variant of $MnGa_2S_4$ (e). These patterns can be compared with the experimentally observed ones, shown in Fig. 3.

tions were also suggested from X-ray powder diffraction studies (*8*).

The diffraction patterns of Fig. 3 can all be indexed using a similar monoclinic unit cell, derived from α-Ga_2S_3. The indexing of the superreflections is shown in Fig. 4 (only one orientation variant). From these diffraction patterns the unit cell can be derived. Note that the monoclinic parameter a_m changes upon composition, whereas b_m, c_m, and β (=140°) remain unaltered. The unit cell dimensions (and structures) being related, it is possible to present a structural building principle that describes the structures. It is based on a stacking of metal atom $(\bar{1}2.4) = (100)_m$ planes in the hcp matrix of sulfur atoms. For α-Ga_2S_3 this stacking is *–Ga–Ga–*–Ga–Ga–* etc. (*11, 12*) (see also Fig. 1). For the composition $MnGa_2S_4$, Mn planes have to be introduced in agreement with the Ga/Mn ratio: Mn–Ga–*–Ga–Mn–Ga–*–Ga–Mn– . . . Other compositions can be formed by varying the number of Mn-planes: Mn–Ga–*–Ga–Ga–*–Ga–Mn is $MnGa_4S_7$. This building principle is shown schematically in Fig. 5. It is now possible to derive the ideal atom positions (based on Wurtzite) for Mn, Ga, and *; these were used to simulate the diffraction patterns shown schematically in Figs. 4c and d.

The calculated diffraction patterns for the proposed models fit very well with the observed ones; so the diffraction patterns in Fig. 3 are all composed of the basic diffraction patterns as depicted in Fig. 4. For example, Fig. 3b is composed of three patterns: Fig. 4a and two orientation variants of Fig. 4c. In Table I the unit cell dimensions (derived from the diffraction patterns) together with the $d(200)$ (monoclinic) lattice spacings are collected as a function of composition and periodicity (n) in the diffraction pattern.

The drawings for the Ga_2S_3 and the $MnGa_2S_4$ (Figs. 1 and 6a, respectively) structures were made using these atom positions. In Fig. 6a the alternative monoclinic unit cell has also been indicated. Figures 6b and c show the b_m-projections of

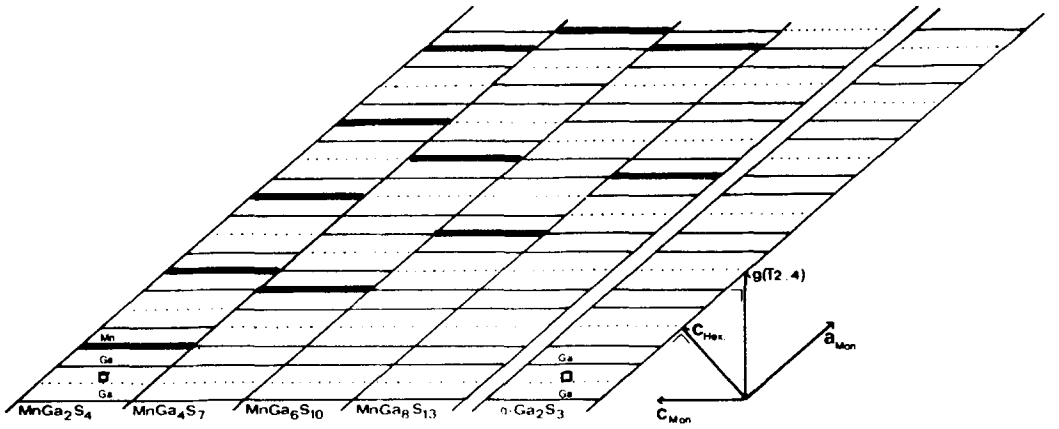

FIG. 5. Schematic representation of stacking of Mn, Ga, and vacancy $(100)_m = (\bar{1}2.4)$ layers. By varying the stacking, maintaining Ga–vacancy–Ga units, different compositions can be derived.

$MnGa_4S_7$ and $MnGa_6S_{10}$. The stacking scheme (Fig. 5) allows to calculate that the observable lattice spacing for a composition $MnGa_8S_{13}$ is 1.5 nm (see Table I). Indeed this lattice spacing was found in some small domains; however, since the domains are very small it is not possible to observe the corresponding superreflections in the diffraction patterns of Fig. 3e. When the domain size is small, rows of superreflections from other orientation variants will intersect the Ewald sphere. The diffuse extra spots which are clearly evident in Fig. 3d can be explained in this manner.

6. High-Resolution Microscopy and Image Computation

In order to obtain more detailed information on the microstructural aspects of these compounds a high-resolution study was performed on different xMnS/$y$$Ga_2S_3$ samples in both the [01.0] and [00.1] orientations, by the use of a JEM 200 CX high-resolution electron microscope. Mostly the regions which were sufficiently thin for obtaining high-resolution images were also rather small; especially the [01.0] section was hard to find because of the low tilting capabilities (±10°). Another experimental problem was caused by the radiation sensitivity of the materials; after about 15 min of observation most of the crystals appeared to be severely damaged by the high-intensity electron beam. Specimen orientation and microscope adjustments had to be performed very fast.

6.1. *The [01.0] Orientation*

Figure 7 shows a region of $MnGa_4S_7$ at a total magnification of 5×10^6. The lattice spacings measured on this micrograph match fairly well with the ones deduced from the electron diffraction patterns. Between the dark parallel lines pairs of white dots are visible which possibly correspond to the arrangement of the vacant tetrahedra

TABLE I

DIMENSIONS OF THE MONOCLINIC a AXIS AND d_{200} FOR DIFFERENT VALUES OF n IN NANOMETERS

n	Composition	a (monoclinic)	$d_{200} = n \cdot d_{\bar{1}2.4}$[a]
3	Ga_2S_3	1.107	0.350
4	$MnGa_2S_4$	1.476	0.467
7	$MnGa_4S_7$	2.583	0.817
10	$MnGa_6S_{10}$	3.690	1.167
13	$MnGa_8S_{13}$	4.797	1.517

[a] Value $d_{\bar{1}2.4} = 0.1167$ nm.

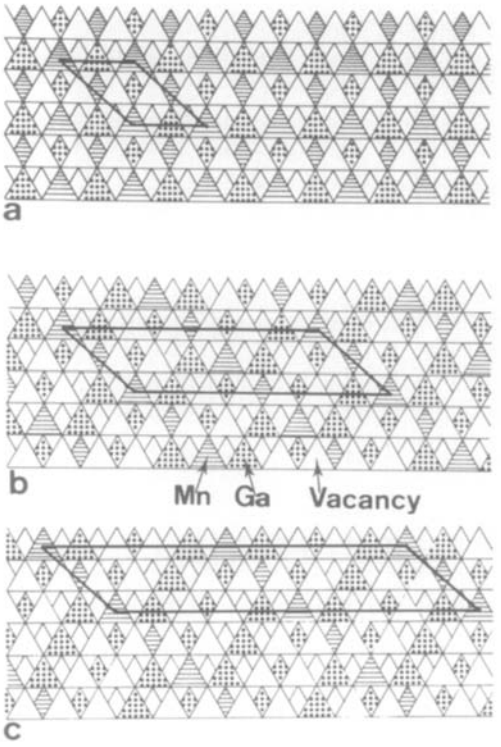

FIG. 6. The [01.0] projections of the structures of (a) $MnGa_2S_4$, (b) $MnGa_4S_7$, (c) $MnGa_6S_{10}$. Note that, according to Table I, the length of the a_m axis in (c) is two times as large as that of the smallest monoclinic unit cell.

in the structure. The diffracted beams used to obtain this image are encircled in the inset.

If the ratio x/y is between 1/2 and 1/3 the system tends to adopt a stable structure with a composition somewhere between that of $MnGa_4S_7$ and $MnGa_6S_{10}$. This can be observed in Fig. 8; thin slabs of both compositions alternate in an almost regular way as indicated ((2) stands for $MnGa_4S_7$, (3) for $MnGa_6S_{10}$). This picture clearly demonstrates that on a microscale the system remains stoichiometric; the nonstoichiometry which is found most of the time in a chemical analysis of these specimens is entirely due to a stacking of building-blocks in a certain order while the blocks themselves have a definite composition.

6.2. The [00.1] Orientation

In the [00.1] orientation we should be able to observe how the sulfur tetrahedra in the basal plane are filled with Mn and Ga and also how the vacancies are ordered. We expect to find a different intensity for each kind of tetrahedron. However, intuitively it is clear that since Ga and Mn have almost equal electron-scattering factors, the contribution of both atoms to the overall scattering process will be almost the same, so we do not expect to be able to observe any difference between the images of Ga- and Mn-filled tetrahedra.

Also on an intuitive basis we can try to predict the general character of the [00.1]-oriented high-resolution pictures; therefore it is convenient to draw the structure models in a c_h-projection as in Fig. 9 where only one basal plane is shown. Taking into account the hexagonal stacking of the sulfur (00.1) layers and the fact that the superstructure axis c_m is not parallel to c_h we find that not all of the compounds are equally well suited for high-resolution imaging and image simulations; this means, for instance, that for $MnGa_6S_{10}$ the unit cell parameter along the c_h axis is about 2.4 nm which certainly will give rise to upper-layer-line interactions. In order to avoid these problems (which are difficult to handle in image simulations as yet) we have chosen the simplest structure ($MnGa_2S_4$) for comparison of real images with image simulations and to constitute in this way some kind of imaging code. If we draw a [00.1] projection of the heavy atoms only for the structure of $MnGa_2S_4$ we find some kind of wave-like atom strings parallel to the a_h axis (see Fig. 12, left side). We expect to find such a pattern in some of the electron micrographs of through-focal series.

Using the atom parameters derived in the previous section, image calculations were performed using the real-space method; this method is an improved version of the

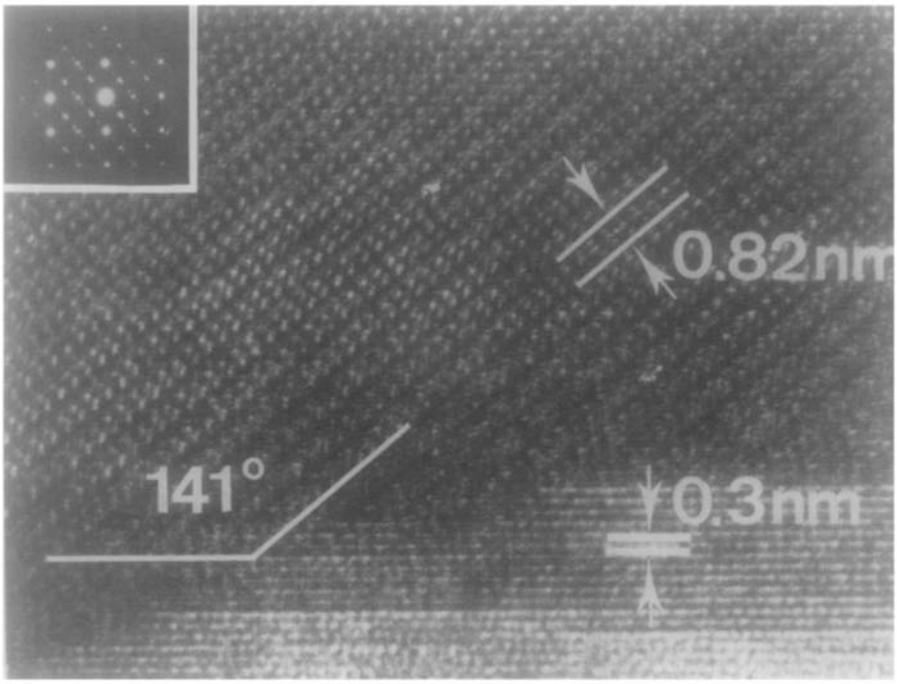

FIG. 7. High-resolution micrograph of a region of $MnGa_4S_7$. The 0.3-nm lattice spacing of the basal planes is clearly visible.

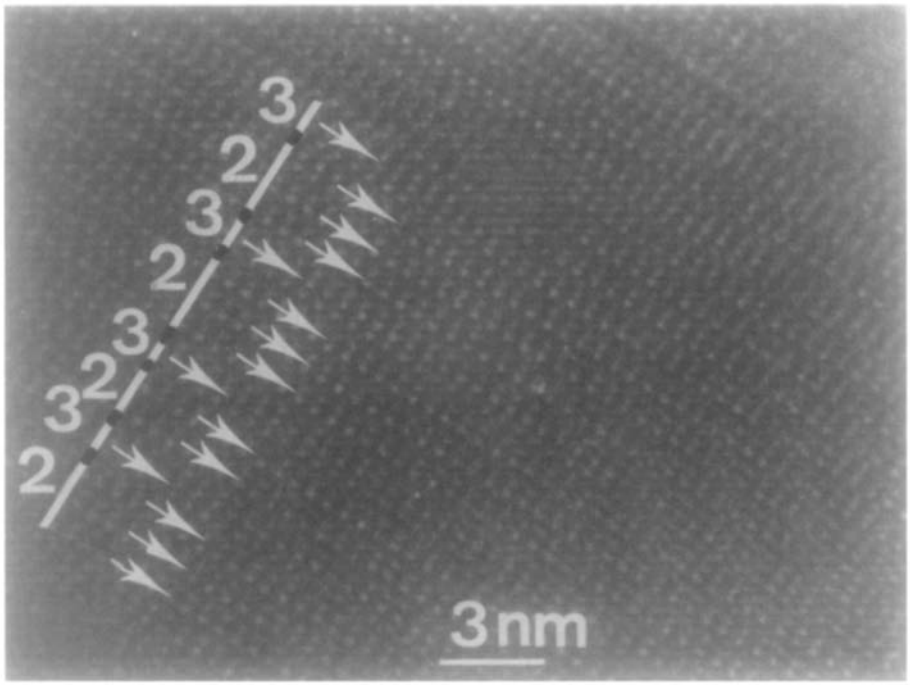

FIG. 8. High-resolution micrograph of an almost regular alternation of thin slabs of $MnGa_4S_7$ (2) and $MnGa_6S_{10}$ (3).

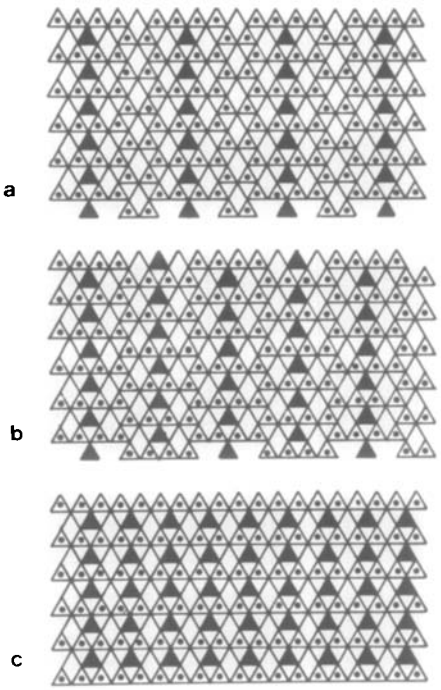

FIG. 9. The [00.1] projections of one basal plane of (a) $MnGa_6S_{10}$, (b) $MnGa_4S_7$, and (c) $MnGa_2S_4$. Ga-filled tetrahedra are represented by dotted triangles while black triangles correspond to Mn-filled tetrahedra.

multi-slice method in which the electron propagation between the slices is computed in real space instead of in reciprocal space, thereby decreasing the calculation time (*14*). The results of this simulation are shown in Fig. 10 (image intensity as a function of crystal thickness and microscope defocus value for the [00.1] orientation of $MnGa_2S_4$). A manganese atom is placed in the lower left corner. Note that in most pictures the expected wave-like patterns are clearly visible.

Figure 11a shows a high-resolution image of a region with composition $MnGa_2S_4$ viewed along the hexagonal *c*-axis. Clearly the unit cell is of the orthorhombic type; at present however it is not yet obvious which of the white dots should be interpreted as corresponding, e.g., to the Mn-filled tetrahedra. Figure 11b is an image of another region taken with a different defocus; the orthorhombic cell remains visible but the contrast has completely reversed. All the white dots are replaced by black ones.

When one concentrates on the symmetry properties of these micrographs one finds that the projected space group is not the same as that of the proposed structure model; since it is well known that the symmetry of axial high-resolution images must be at least that of the projected crystal potential (*15*) one has to conclude that either the structure model is wrong or the specimen (or beam alignment) was inaccurate, giving rise to a symmetry change in the high-resolution pictures (*16*).

Suppose that our structure model is not correct, i.e., the superstructure positions are wrong. It is important to note that, first, the Wurtzite-type reflections in the electron diffraction patterns are very sharply defined and, second, that the symmetry of Fig. 11a corresponds to that of Fig. 9a which is a projection of one basal plane only. This leads us to the following conclusion: the basic sulfur lattice is indeed a hexagonal close-packed lattice and the superstructure within one basal plane is correctly given by our first structure model. The only possibility left is that the stacking sequence of the superstructure along the [00.1] direction is not the one we proposed.

For our structure considerations and image simulations it appears more convenient to work with an orthorhombic unit cell, instead of a monoclinic one; since the b_0 lattice parameter is twice a_h we have two possibilities of stacking the superstructure atoms along the hexagonal *c*-axis: the first one was already described in a previous section, and the second one can be derived from the first by applying to each B-layer a displacement vector $\mathbf{R} = 1/2[100]_o = [01.0]$. This is illustrated in Fig. 12a where it represents a projection of the heavy atoms in the unit cell; in the lower part of the figure the wave-like atom strings are indicated. In

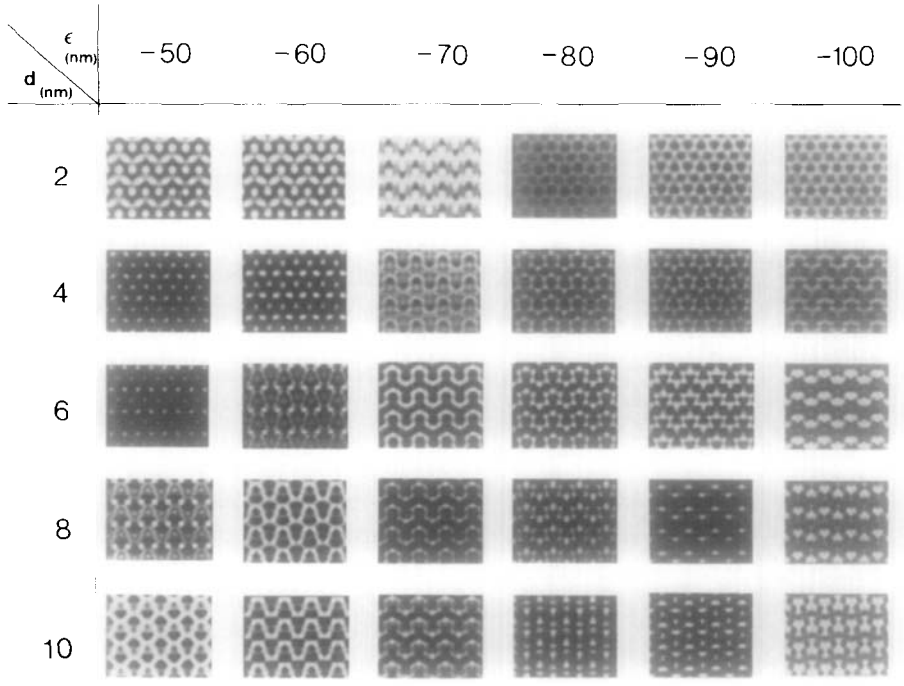

FIG. 10. Simulation of the image intensity as a function of crystal thickness and microscope defocus value for the [00.1] orientation of $MnGa_2S_4$.

Fig. 12b the new structure is shown, which has the same unit cell dimensions. Since the point-resolution of the JEM 200 CX high-resolution electron microscope is about 0.26 nm and the distance between, e.g., two Mn atoms in projection only about 0.2 nm we cannot expect to separate the "columns" of Mn, Ga, or vacancies in the images; two columns will be seen as one bright or dark spot as indicated schematically in Fig. 12b by the shaded regions in the bottom part. The symmetry of this projection matches very well the experimentally observed symmetry.

Image calculations for the new structure model were performed and they are in good agreement with the experimental results, as can be seen in a through focus series in Fig.

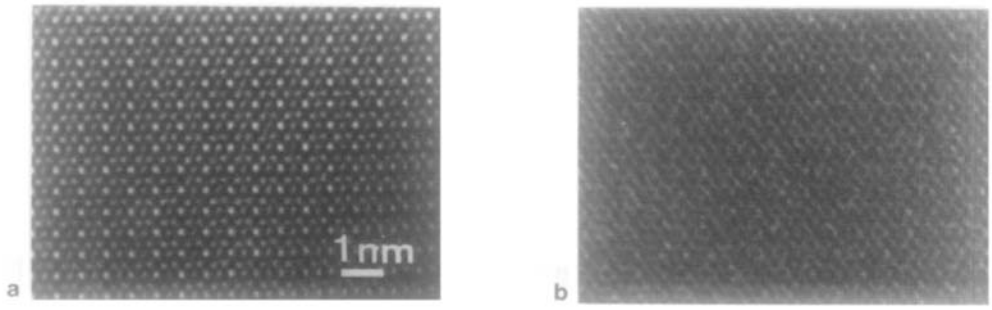

FIG. 11. (a),(b) High-resolution electron micrographs of $MnGa_2S_4$ in the [00.1] orientation for different defocus values.

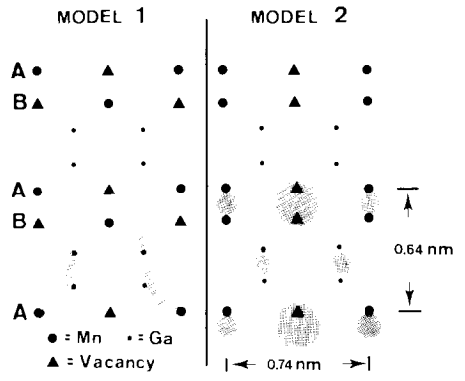

FIG. 12. Projected structure models of $MnGa_2S_4$ (projection axis = c_h) A and B indicate the different basal planes to which the metal atoms belong. Note that sulfur atoms are not shown.

13 (the thickness of the crystal was taken to be 3 nm).

In some crystals we observed both structure variants in a single region; this excludes the possibility that the symmetry change was caused by a crystal misorientation or a beam misalignment. In order to confirm the existence of both structure variants we investigated the [01.0] section of several crystal fragments. Figure 14 shows some high-resolution micrographs of the [01.0] section of $MnGa_2S_4$ with image simulations in the insets (simulations were carried out for a crystal thickness of 10 nm). Figures 14a and b correspond to the new structure model, Figs. 14c and d to the old one. The agreement between structure models and observations proves that $MnGa_2S_4$ can exist in two structure variants, that are equally possible since the sulfur tetrahedra share only corners in both models.

In the structures with a lower Mn content there are correspondingly more possibilities of stacking the different basal planes, so there the question remains which modification or variant will be most likely. This will be further investigated.

7. Generalization of the Structure Model

The electron-microscope results show that substantial disorder (in form of domains and planar defects) can occur in several nMnS · Ga_2S_3 compounds.

Figure 5 clearly shows that without changes in the sulfur lattice a Mn layer can change into a vacancy or Ga layer, the interface being along the (00.1) plane. This explains very well the two observed intergrowth features: orientation variant forma-

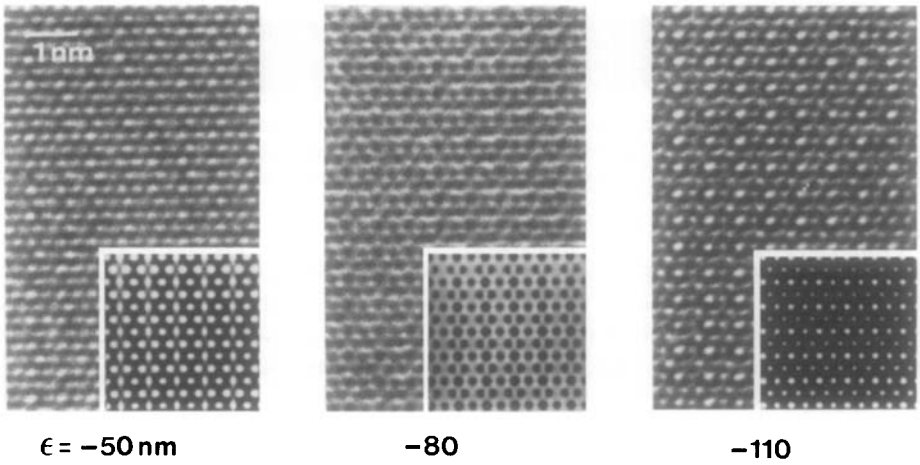

FIG. 13. Through focal series and image simulations for $MnGa_2S_4$ according to the second structure model. The defocus value is indicated. The crystal thickness was taken to be about 3 nm.

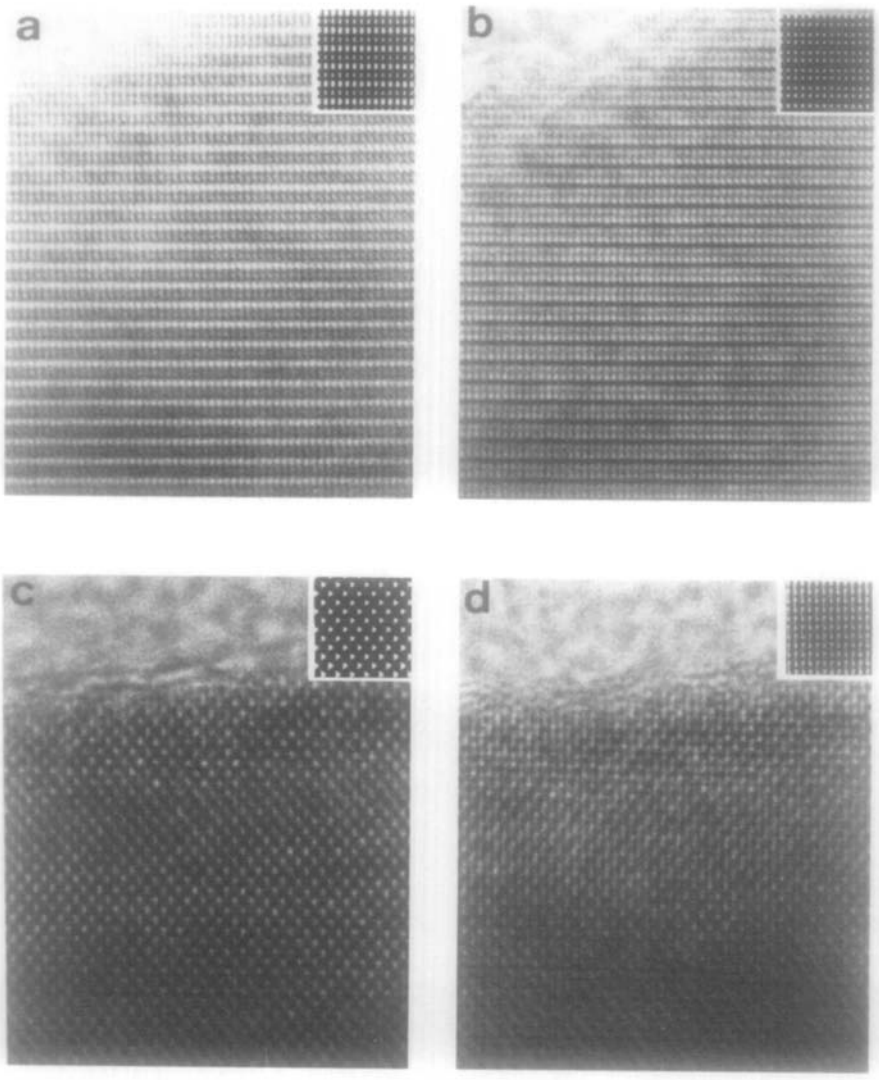

FIG. 14. High-resolution electron micrographs of two regions of a small crystal fragment; (a) and (b) show a good correspondence with the image simulations (shown in the inset) based on the second structure model while (c) and (d) show micrographs and simulations based on the first structure model.

tion of the compounds nMnS · Ga_2S_3 and orientation variant formation of one compound within the basic structure of the others like Ga_2S_3 and $MnGa_2S_4$ (see Fig. 8).

The apparent possibility of planar disorder suggests that a more generalized description of the structure model in terms of extended defects is possible. Comparison of the proposed structures of the different compounds studied reveals that they can all be derived from the structure of α-Ga_2S_3 by regular introduction of defect planes in the metal atom lattice of the structure (Fig. 6). The Mn atoms are located in these defect planes, so the coordination of the S atoms in the defect plane becomes "ideal," 2 $Ga^{(3ve)}$ + 1 $Mn^{(2ve)}$ + 1 vacancy. (The number of electrons available for a S atom was 2

$\times \frac{3}{4} = 1.5$ now becomes $2 \times \frac{3}{4} + \frac{2}{4} = 2$). The introduction of the Mn-planes in the Ga_2S_3 thus has a stabilizing effect since the number of "badly surrounded" S atoms is reduced. Figure 15 which shows the basal plane arrangement of filled tetrahedra represented by triangles, emphasizes that by the introduction of Mn planes between two mirror-related Ga_2S_3 slabs, a continuous change from the Ga_2S_3 structure to the $MnGa_2S_4$ structure is possible. The dotted lines are the traces of the defect planes which actually go through the complete stacking of the tetrahedral layers. For the first structure model the defect plane is inclined to the basal plane by an angle of 140°(=β). The interface between two slabs is the (12.4) or $(100)_m$ plane. For the second structure model the defect plane is perpendicular to the basal plane. The [01.0] diffraction pattern of $MnGa_2S_4$ (second variant) was simulated and is shown in Fig. 4e. The forbidden reflections in the space group *Cc* which are clearly visible in Figs 3d and e can be explained by the presence of this variant. By the regular introduction of "Mn defect planes" a new homologous series of structures is derived: $nGa_2S_3 \cdot MnS$ with $n = \infty, \ldots 4,3,2,1$, for which the repeat distance of the defect planes of course determines the unit cell dimensions. Only the a_m axis changes in length upon changes in the Ga/Mn ratio. (It still remains to be examined whether this change also occurs in the structures with $n > 2$ that are based on the second model, i.e., in which the defect plane is perpendicular to the basal sulfur plane.) The described defect plane is clearly nonconservative since its introduction in the structure is accompanied by a composition change. Such a defect plane could be described as "chemical anti-phase boundary" or "chemical twin plane." The latter is perhaps the best name, as within the tetrahedral layer (basal plane) the Ga_2S_3 slabs are mirror-related while in each second layer the twin planes are translated with respect to the previous layer: the result being that the twin-composition boundary (where the structural slabs meet) and the twin plane $(100)_m$, do not coincide: a chemical twin plane. For the second structure model the twin plane has the coherent orientation. Since both structure variants are observed, sometimes in the same crystal, the twin plane can change its character (i.e., from coherent to incoherent and vice versa). Essential is the change in stoichiometry caused by the boundary plane justifying the term of "chemical."

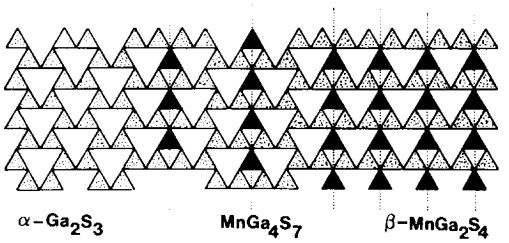

FIG. 15. Schematic representation of the hcp basal plane. Tetrahedral sites are represented by triangles. Dotted triangles correspond to Ga tetrahedra and black triangles to Mn tetrahedra. The dotted lines are the traces of the defect planes. By varying the distance between these defect planes the composition is varied also. The defect planes make an angle of 140° with the basal plane in the first model while in the second they are perpendicular to it.

8. Conclusion and General Considerations

Electron microscopy has proved to be a useful tool in finding a structural explanation for the observed nonstoichiometry, the additional phases and the disorder in the compounds $xMnS/yGa_2S_3$. Symmetry considerations allowed us to derive a new structure variant of $MnGa_2S_4$. The building principle is based on the structure of α-Ga_2S_3 in which upon substitution of MnS in the Ga_2S_3 matrix chemical twin planes are formed (coherent in the second model), which are however restricted to a specific area. This defect plane, if introduced periodically in Ga_2S_3, results in a new homolo-

gous series of compounds $n\mathrm{Ga_2S_3} \cdot \mathrm{MnS}$ ($n = \infty, \ldots, 4,3,2,1$) for which so far the members 4,3,2,1 have been identified using electron microscopy. These compounds often occur as small domains within a host structure, or as a conglomeration of orientation variants within the hcp sulfur matrix. The number of compounds in this series can perhaps be expanded by suitable preparation techniques. The solubility of MnS in $\mathrm{Ga_2S_3}$ appears to be the result of intergrowth of small new phase domains in the $\mathrm{Ga_2S_3}$ matrix. The actual composition within a domain is accommodated by the concentration and type of defect planes while the observed disorder is the result of irregularities in the period of the extended defects. There is strong evidence that a third modification of $\mathrm{Ga_2S_3}$ exists which has a structure comparable to α-$\mathrm{Ga_2S_3}$ (the same metal– atom–vacancy ordering) but which is slightly distorted (space group $C2$ or Cm). However, the forbidden $l = odd$ reflections can also be explained by the presence of very small areas in which the stacking of the metal atoms is that of the second structure model.

From the results of the previous section the following general conclusions can be made.

The defect plane observed in compounds $x\mathrm{MnS}/y\mathrm{Ga_2S_3}$ shows some similarities with the concept of the Crystallographic Shear plane (*17*); the cation–vacancy concentration reduces by a controlled filling of the available tetrahedral sites in the Wurtzite structure. Of course the S-coordination polyhedron also changes. Note that the linkage between the tetrahedra does not change. The fact that a fairly large number of defect-plane-derived superstructures are formed in the system $n\mathrm{Ga_2S_3} \cdot \mathrm{MnS}$, and the observation that in some crystals there is often a small-scale repeat over large distances (we observed a repeat of 5.5 nm, corresponding to $n = 11$) suggests that the interaction between the incoherent twin planes is repulsive. However, from the results in Section 8.1 it cannot be established to which distance this repulsion extends, i.e., whether or not additional members of the homologous series occur.

It may seem that the described twinning model is more generally applicable in explaining nonstoichiometry and disorder in defect tetrahedral structures. Comparison of the structures of β-$\mathrm{MnGa_2S_4}$ and β-$\mathrm{ZnAl_2S_4}$ suggests that the latter structure model should be reconsidered because microstructural variations such as domain formation, anti-phase boundaries, and perhaps nonstoichiometry (solubility of $\mathrm{Al_2S_3}$ in $\mathrm{ZnAl_2S_4}$?) might have resulted in structural artifacts due to the method of investigation (X-ray powder diffraction (*10*)).

Furthermore as there is no indication that the twinning is specific for hcp tetrahedral compounds, it is likely that it can also account for nonstoichiometry in tetrahedral compounds with structures based on the Blende type, for example, in the system $\mathrm{Ga_2S_3}$/FeSe (*18*).

References

1. L. A. Bursill and B. G. Hyde, *in* "Progress in Solid State Chemistry" (H. Reiss and J. O. McCaldin, Eds.), Vol. 7, pp. 177–253, Pergamon, Oxford (1972).
2. B. G. Hyde, A. N. Bagshaw, S. Andersson, and M. O'Keefe, *Annu. Rev. Mater. Sci.* **4,** 43 (1974).
3. A. E. Van Arkel, *Chem. Weekbl.* **5,** 41 (1965).
4. E. Parthe, "Cristallochimie des structures tetrahedriques," Trad. J. Coing-Boyat, Gordon & Breach, Paris (1972).
5. M. Bakker, Ph.D. thesis, Rijksuniversiteit Leiden, Holland.
6. R. W. G. Wyckoff, "Crystal Structures," 2nd ed., Vol. 1, p. 108, Interscience, New York (1963).
7. P. Viswanadham and J. G. Edwards, *Mater. Res. Bull.* **8,** 1079 (1973).
8. M. P. Pardo, P. H. Fourcroy, and J. Flahaut, *Mater. Res. Bull.* **10,** 665 (1975).
9. L. Dogguy-Smiri, N. H. Dung, and M. P. Pardo, *Mater. Res. Bull.* **13,** 661 (1978).

10. G. A. STEIGMANN, *Acta Crystallogr.* **23,** 142 (1967).
11. J. GOODYEAR, W. J. DUFFIN, AND G. A. STEIGMANN, *Acta Crystallogr.* **14,** 1168 (1961).
12. G. COLLIN, J. FLAHAUT, M. GUITTARD, AND A. LOIRREAU-LOZACH, *Mater. Res. Bull.* **11,** 258 (1976).
13. H. HAHN AND G. FRANK, *Anorg. Allg. Chem.* **278,** 333 (1955).
14. D. VAN DYCK, *J. Microsc.* **119,** 141 (1980).
15. B. F. BUXTON, J. A. EADES, J. W. STEEDS, AND G. M. RACKHAM, *Philos. Trans. Soc., London* **281,** 171 (1975).
16. D. J. SMITH, W. O. SAXTON, M. A. O'KEEFE, G. J. WOOD, AND W. M. STOBBS, *Ultramicroscopy* **11,** 263 (1983).
17. L. A. BURSILL AND B. G. HYDE, *Prog. Solid State Chem.* **7,** 177 (1972).
18. M. P. PARDO AND J. FLAHAUT, *Mater. Res. Bull.* **15,** 1043 (1980).